The Company of Biologists

METHODS & TECHNIQUES

Simultaneous measurement of 3D zooplankton trajectories and surrounding fluid velocity field in complex flows

Deepak Adhikari[1],[*],[‡], Brad J. Gemmell[2], Michael P. Hallberg[1], Ellen K. Longmire[1] and Edward J. Buskey[2]

ABSTRACT

We describe an automated, volumetric particle image velocimetry (PIV) and tracking method that measures time-resolved, 3D zooplankton trajectories and surrounding volumetric fluid velocity fields simultaneously and non-intrusively. The method is demonstrated for groups of copepods flowing past a wall-mounted cylinder. We show that copepods execute escape responses when subjected to a strain rate threshold upstream of a cylinder, but the same threshold range elicits no escape responses in the turbulent wake downstream. The method was also used to document the instantaneous slip velocity of zooplankton and the resulting differences in trajectory between zooplankton and non-inertial fluid particles in the unsteady wake flow, showing the method's capability to quantify drift for both passive and motile organisms in turbulent environments. Applications of the method extend to any group of organisms interacting with the surrounding fluid environment, where organism location, larger-scale eddies and smaller-scale fluid deformation rates can all be tracked and analyzed.

KEY WORDS: Tomographic PIV, 3D PTV, Infrared, Turbulence–organism interaction, Plankton drift

INTRODUCTION

Interactions between organisms and complex flow fields are of significant consequence to many ecological processes (e.g. predator–prey interactions, swimming behavior, spatial dispersion and distribution, diel migration). Thus, turbulence–organism interactions have received much recent attention (e.g. Prairie et al., 2012; Guasto et al., 2012; Durham et al., 2013; Jumars et al., 2009; Yamazaki and Squires, 1996). Quantifying turbulent flow fields with high spatial and temporal resolution, and relating them to the behavior and distributions of organisms, e.g. zooplankton, is critical for advancing our understanding. However, obtaining such data is challenging. First, both turbulent flows and planktonic motion are unsteady and three-dimensional, requiring a time-resolved, volumetric measurement system; second, plankton can propel themselves relative to the surrounding fluid leading to local differences in fluid and organism velocity; and third, many planktonic organisms have transparent/translucent bodies, making it challenging to locate and track them relative to both small-scale fluid elements as well as larger-scale eddies. Measurements of both smaller-scale turbulence–plankton

interactions and resulting larger-scale plankton trajectories and spatial distributions are necessary to develop accurate models of organism–flow interactions. This motivates the current efforts to implement a non-intrusive automated volumetric measurement technique capable of capturing interactions over a range of length scales.

Consider calanoid copepods (size ~1 mm) interacting with oceanic flow. Copepods account for ~80% of all meso-zooplankton biomass in the ocean (Mauchline, 1998) and form key links in aquatic food webs (Woodson et al., 2014; Miller, 2004). In uniform flow, these copepods typically drift with the fluid. When hydrodynamic perturbations are detected, however, they can execute sudden escape 'jumps' reaching speeds up to $0.5\ \mathrm{m\ s^{-1}}$ (Yen, 2000). Previous studies indicate that copepods respond to local fluid velocity gradients (Fields and Yen, 1997; Kiørboe et al., 1999; Buskey et al., 2002; Adhikari, 2013), although sustained turbulence can hinder this response (Gilbert and Buskey, 2005; Robinson et al., 2007).

Techniques used to estimate fluid velocity gradients sensed by copepods have included: (1) potential flow equations (e.g. Haury et al., 1980; Buskey et al., 2002); (2) manual 2D particle tracking in laminar flows (e.g. Kiørboe et al., 1999); and (3) planar particle image velocimetry (PIV) (Woodson et al., 2005). Techniques 1 and 2 do not work in turbulent or complex flow fields. Although technique 3 can measure in-plane velocity gradients in complex flows, motions of both copepods and the fluid are inherently three-dimensional, and planar imaging methods cannot capture out-of-plane fluid velocity gradients or organism trajectories. PIV employing visible pulsed laser light may also be problematic because many plankton are phototactic. Thus it may be necessary to operate any pulsed illumination at wavelengths beyond the organisms' detection limit (e.g. infrared).

Digital holography, volumetric three-component velocimetry (V3V) and tomographic PIV all yield fluid velocity measurements in 3D space. Digital holography has been applied to track a copepod feeding current (Malkiel et al., 2003) and copepod nauplius kinematics (Gemmell et al., 2013). V3V has been used to study fish (Flammang et al., 2011) and jellyfish (Gemmell et al., 2015) locomotion. Tomographic PIV has been used to study wakes of swimming copepods (Murphy et al., 2012) and swimming Daphnia (Michaelis, 2014). These studies observed only a single organism, which was typically identified and tracked manually. Recently, a fish–copepod interaction was investigated in a quiescent tank using tomographic PIV (Adhikari and Longmire, 2013; Gemmell et al., 2014). Although fish location and tracking were automated, the copepod was difficult to distinguish from the surrounding tracer particles and had to be identified manually. Organism identification becomes more challenging as the field of view increases in size and the organisms occupy smaller areas within image fields. Thus, this single-wavelength technique was impractical for identifying and tracking multiple copepods in a complex flow.

[1]Department of Aerospace Engineering and Mechanics, University of Minnesota, Minneapolis, MN 55455, USA. [2]Marine Science Institute, University of Texas at Austin, Port Aransas, TX 78373, USA.
*Present address: School of Civil and Environmental Engineering, Georgia Institute of Technology, Atlanta, GA 30339, USA.

‡Author for correspondence (deepak.adhikari@ce.gatech.edu)

Journal of Experimental Biology

We introduce here a combined tomographic PIV and 3D particle tracking velocimetry (PTV) technique based on two light sources to study turbulence–copepod interactions over a range of length scales. Tomographic PIV based on pulsed infrared light measures time-resolved fluid velocity on a volumetric Cartesian grid, whereas 3D PTV based on a steady white light source independently and automatically identifies and tracks discrete organisms within the same measurement volume without eliciting phototactic responses. This technique resolves small-scale interactions by determining the location and velocity of plankton as well as local fluid velocity gradients. At the same time, it provides plankton trajectories, plankton spatial distribution and fluid velocity variations over larger length scales. We demonstrate the method by determining copepod trajectories and local strain rates both upstream and downstream of a cylinder in cross flow where the flow in the downstream region is highly unsteady and three-dimensional. In addition, we illustrate the capability to extract zooplankton slip velocity such that, even for these small organisms, their drifting trajectory in unsteady flow can be different from those of fluid particles.

MATERIALS AND METHODS
The experiments were conducted at the University of Texas Marine Science Institute at Port Aransas, TX.

Species
The copepods examined were *Acartia tonsa* Dana 1849 (size ~1 mm) collected from Mustang Island, Texas (27°48′N, 97°05′W). The collected water sample was filtered through a 2000 µm mesh to remove debris and larger organisms. A fiber optic source light was used to attract the copepods. The surrounding water was collected, and *A. tonsa* were sorted from other zooplankton using a wide bore pipette and stereo microscope before being transferred to the water channel.

Measurement setup
Fig. 1 shows the setup applied to measure fluid motion and zooplankton distribution. For tomographic PIV, the measurement volume was illuminated with an Oxford Firefly infrared laser (wavelength: 808 nm) with 3 mJ pulse^{-1} and pulse duration of 10 µs. As plankton and fish are insensitive to this wavelength (Adhikari and Longmire, 2013), the illumination did not affect their behavior. The beam was expanded into a sheet with spanwise thickness ~20 mm. The channel was seeded with 55 µm polyamide particles (including 11% titanium dioxide by weight). Four high-speed cameras (1280×800 pixels), each fitted with a 105 mm Nikon Micro-Nikkor lens and infrared-pass optical filter, were aimed at the measurement volume. Scheimpflug mounts (LaVision, model no. 1108196) were used to ensure that each camera image was in focus. The infrared-pass filters allowed only the infrared illumination scattered from the tracer particles and copepods to pass through the lens, where the copepod scattering was comparatively weak. Although water strongly attenuates IR wavelengths, limited distance of laser propagation through water (20 cm), the laser pulse energy, choice of particles, and camera sensitivity yielded scattering intensity sufficient for high quality PIV images. The cameras were placed in a 'square' configuration, and tilted approximately 30 deg to the z-axis. In the test section, the x-axis (horizontal) and y-axis (vertical) are defined parallel to the laser sheet, and the z-axis is defined positive towards the cameras.

For 3D PTV, the same measurement volume was illuminated simultaneously with two white LED lamps configured for dark-field illumination. The lamps were angled at about 60 deg to the negative z-axis (Fig. 1) and tilted slightly towards the negative y-axis. Since the laboratory was well lit, and the white lamps continuously illuminated a broad volume across the test section, copepods did not exhibit phototactic behavior. Two additional high-speed cameras (1280×800 pixels), fitted with 105 mm Micro-Nikkor lenses and infrared-blocking optical filters, were aimed at the measurement volume in a top–bottom configuration to view the zooplankton. The cameras were tilted at 30 deg to the z-axis. The LED lamps and infrared-blocking filters were effective at illuminating the zooplankton but not the smaller tracer particles. Image acquisition was synchronized by supplying the
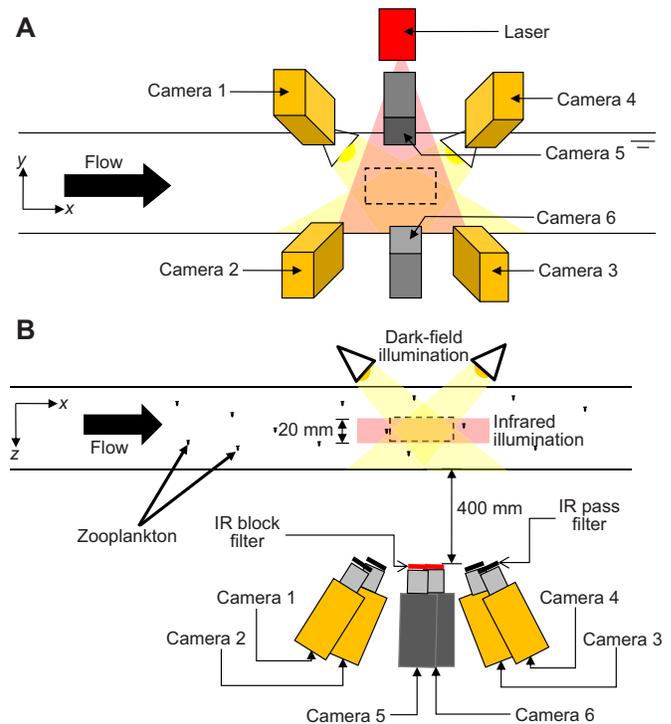
Fig. 1. Schematic of the simultaneous tomographic PIV and 3D PTV measurement system. Cameras 1–4 (orange) acquire tomographic PIV images and cameras 5 and 6 (gray) acquire 3D PTV images. Dashed box within the infrared illumination represents the measurement volume. The LED lamps in dark-field configuration are angled downwards in the x-y plane, and inwards in the x-z plane.

frame signal from one master camera to the other five cameras and the laser. All cameras recorded at the laser pulse frequency of 330 Hz.

Methodology
Images were processed with LaVision DaVis 8.0 software. A calibration plate was traversed to nine positions across the measurement volume depth, and a preliminary mapping function for all six cameras was determined from the resulting image sets. A self-calibration procedure minimized disparity errors and hence corrected the calibration mapping function for all cameras leading to a reduced calibration error (Wieneke, 2008). Readers are referred to Scarano (2013) and Maas et al. (1993) for complete descriptions of tomographic PIV and 3D PTV, respectively. For tomographic PIV, images were first processed with a sliding minimum convolution filter with 5×5 pixel window to eliminate background noise. Then, the images were normalized with a reference image to compensate for larger-scale variations in background intensity. This pre-processing ensured good reconstruction quality of the particles. Volumetric fields of particle intensity were reconstructed using the MLOS-SMART algorithm (Atkinson and Soria, 2009). To avoid contaminating local fluid velocity vectors during cross-correlation, all zooplankton were masked from fluid measurement volumes. A cubic mask of 7×7×7 voxels was applied at all zooplankton locations (identified in the PTV images). Cross-correlating masked interrogation volume pairs separated by Δt=3.0 ms yielded fluid velocity fields measuring 80 mm×37.5 mm×19 mm. The smallest interrogation volume yielding high quality results was 48×48×48 voxels. Using a 75% overlap resulted in fields of 88×43×21 vectors with 0.9 mm spacing. Zooplankton image sequences were pre-processed similarly before the 3D PTV operation in Da Vis was applied to triangulate the position of each zooplankton within the overall measurement field of 80 mm×37.5 mm×19 mm. The triangulation search radius was 1 pixel. Zooplankton velocity was obtained by dividing the volumetric displacement by Δt. Sixty-four neighboring grid points were used for least-square Taylor-series interpolation to determine the spatial velocity gradients of fluid flow at the location of a copepod. See Appendix 1 for details on uncertainty.

RESULTS AND DISCUSSION

Figs 2 and 3 illustrate results obtainable from the infrared tomographic PIV+3D PTV measurement technique. Fig. 2A shows copepod trajectories in uniform flow approaching a wall-mounted cylinder. As copepods approach the cylinder, they exhibit 'jumps' characterized by sudden changes in speed and direction. An algorithm was developed to identify the locations at which jumps initiated (denoted by circles). Flow is generated in a closed-loop water channel (see Adhikari, 2013 for details). The measurement fields are well above the bottom boundary layer, such that far upstream of the cylinder, the mean velocity across the field of view is uniform to within 1% (Krizan, 2014). The intensity of velocity fluctuations (u'/U) in this zone is 0.35%, where u' represents the RMS velocity ($u' = \sqrt{\frac{1}{3}(u'^2_{x^2} + u'^2_{y^2} + u'^2_{z^2})}$) and U represents the mean, so that the flow is essentially laminar. Copepods did not jump under those conditions.

Fig. 2B shows an x-z projection of the jump locations. Copepods typically execute three types of jump: (1) escape response from predators; (2) ambush of prey; and (3) repositioning or reorientation hops (Jiang and Kiørboe, 2011). We assume that the jumps in
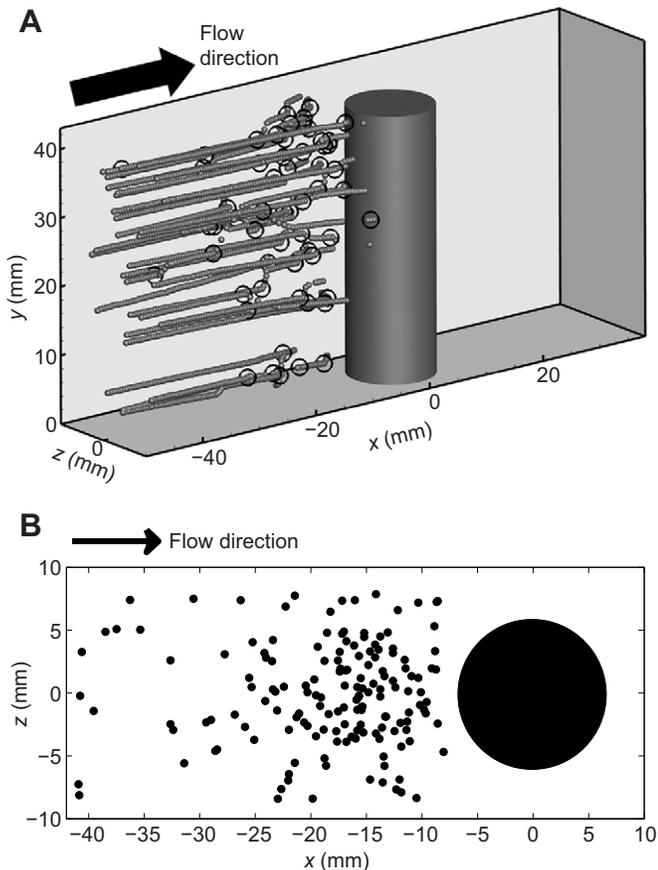
Fig. 2. Copepod trajectories and jump locations upstream of cylinder. (A) Copepod trajectories (black spheres) in uniform flow at 0.077 m s^{-1} approaching a wall-mounted cylinder (diameter: 12.7 mm; cylinder axis: y direction) captured over a time span of 40 s. For clarity, the corresponding volumetric fluid velocity fields are not shown. Circles represent 'jump' locations. Height of the cylinder has been truncated for clarity. (B) x-z projection of jump locations. Black dots represent copepods responding to flow-related disturbances by the cylinder. The cylinder center is located at (x,z)=(0,0) mm. In total, we detected 138 jumps over a period of 120 s (3 sets of 40 s timespan).

Fig. 2B predominantly represent escapes since no prey is present, and the jump location density varies inversely with distance in front of the cylinder. Hence, escapes are triggered by changes in flow quantities as the copepods approach the cylinder.

Fig. 3A shows measurements in the complex wake flow downstream of the cylinder (see Movie 1 for time sequence). Since *Acartia tonsa* exhibit 'hop-and-sink' behaviors (Yen et al., 2008) instead of cruising, the 20 smooth trajectories observed in the wake (Movie 1) indicate that no jumps occurred. Fig. 3B includes a magnified view of a copepod's location where the fluid velocity vector grid is resolved to 0.9 mm, which is comparable to the copepod size. The speed and direction of the copepod differ from those of the local fluid velocity. Since the copepod did not jump in the cylinder wake, this difference must be due to the interactive forces between the copepod and the unsteady flow. Note that this velocity difference did not result from measurement uncertainty (Appendix 1).

Jump locations and hydrodynamic threshold

Copepods are thought to sense flow 'deformation rate' to generate escape jumps. Deformation rate has been commonly calculated as the maximum eigenvalue of the deformation rate tensor or the maximum principal strain rate (MPSR) (Holzman and Wainwright, 2009; Catton et al., 2012; Buskey et al., 2002; Kiørboe et al., 1999; Woodson et al., 2014). MPSR values correlated with *A. tonsa* escape response are 0.5–5 s^{-1} (Kiørboe et al., 1999), 0.4–12 s^{-1} (Buskey et al., 2002) and 1.5 s^{-1} (Fields and Yen, 1997), all in laminar flows. The different values reported result from different ranges present within the flows studied and varying criteria used to characterize the escape response threshold.

Using the fluid velocity fields corresponding with the escapes in Fig. 2, we determined the local MPSR at all escape jump locations. The resulting distribution (Fig. 4, blue) shows that copepods responded to values ranging from 0.25 to 13 s^{-1}, where 80% of the sample responded to the range 0.25–5 s^{-1}. These values are consistent with previous work within the limits of uncertainty (Kiørboe et al., 1999; Buskey et al., 2002; Fields and Yen, 1997). The MPSR distribution at copepod escape locations can be contrasted with the MPSR distribution in the full measurement volume. On average, the escape locations are shifted toward higher MPSR values, and no jumps were observed for MPSR less than 0.25 s^{-1} although such values were frequently present in the flow fields, particularly near the upstream end.

MPSR values were also determined for copepods in the unsteady cylinder wake. Fig. 5 shows MPSR values along copepod trajectories upstream and downstream of the cylinder. The downstream values range from 3 to 10 s^{-1} along the trajectory, yet no escape jump occurred. This intriguing observation, which has never been recorded before, was consistent for more than 9000 copepods measured in the wake for values up to 20 s^{-1}. These MPSR are much higher than those along the upstream trajectory where an escape jump occurred once the MPSR reached 2.2 s^{-1}. The rate of increase in MPSR for the copepod upstream of the cylinder is also highest at 20 s^{-2} when escape was initiated. By contrast, in the cylinder wake, the rate of change of MPSR based on a best polynomial fit to the data in Fig. 5 fluctuates between −30 s^{-2} to 50 s^{-2}, yet no jumps were observed. Thus, the results suggest that depending on the nature of the flow, e.g. laminar versus turbulent, the MPSR threshold value for escape may vary, and there is no simple correlation between rate of increase in MPSR and copepod escape response.
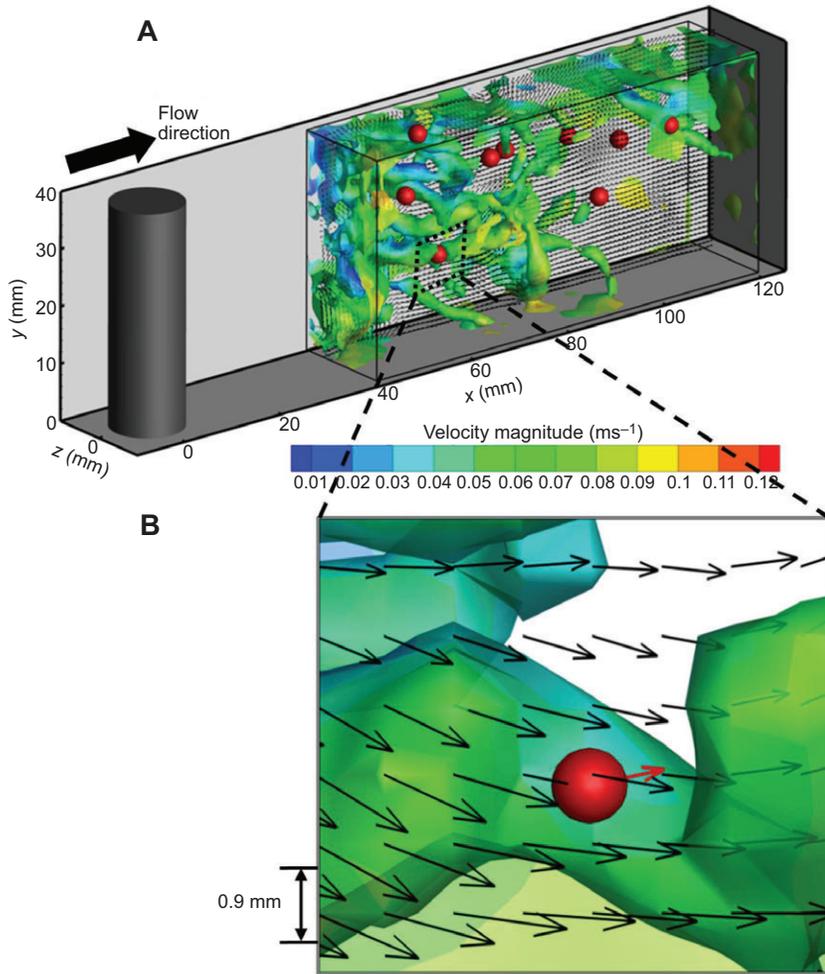
Fig. 3. Volumetric flow field and copepod distribution.
(A) Volumetric flow field and copepod distribution behind a vertically mounted cylinder (diameter: 12.7 mm), located at $(x,z)=(0,0)$ mm. Height of the cylinder has been truncated for clarity. The measurement volume includes both large-scale eddy structures and the spatial distribution of copepods. The vorticity iso-surface is $||\omega||=25$ s^{-1} and the red spheres indicate copepod locations. (B) Zoom-in view of A where copepod velocity (red arrow) differs from surrounding fluid velocity (black arrows).

### Zooplankton trajectories and fluid particle drift in unsteady flow

Slip of an inertial 'point' particle in a fluid can be modeled accurately in the Stokes limit (Maxey and Riley, 1983). However, zooplankton and other organisms typically have finite dimensions, a range of shapes, and variations in density such that their trajectories in complex flows are less predictable. Furthermore, many zooplanktons can self-propel making their trajectory relative to a fluid path line even more complex (Yamazaki and Squires, 1996).

Fig. 6 shows four copepod trajectories in the cylinder wake. None of these copepods jumped. Fluid 'particles' were placed at the initial locations of each copepod and their trajectories were computed by convecting the particles using the local time-resolved fluid velocity.
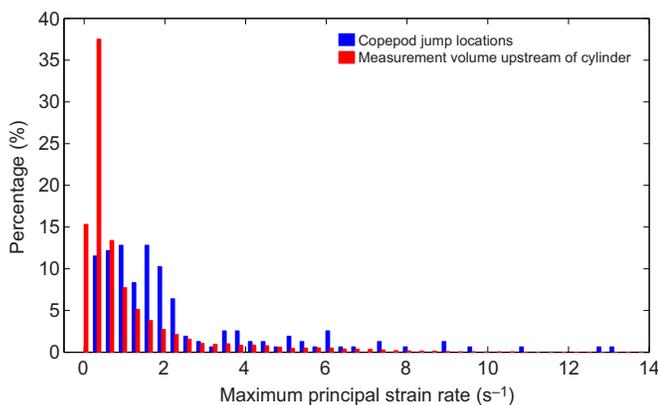
Fig. 4. Distribution of maximum principal strain rate. MPSR measured in fluid at locations where copepod jumps initiated (blue) and throughout the measurement volume upstream of the cylinder (red).
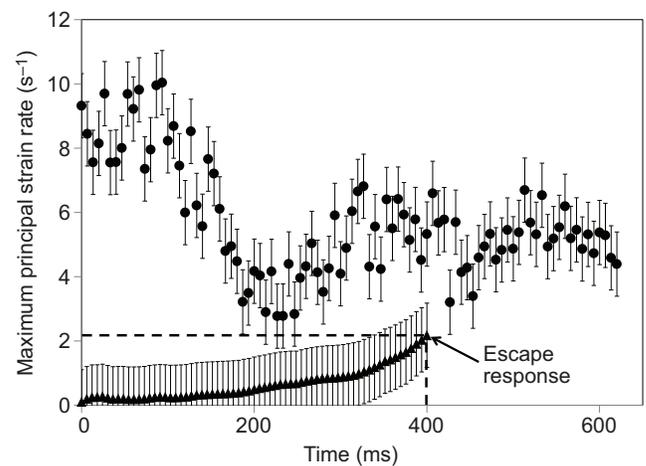
Fig. 5. Maximum principal strain rate experienced by copepods. MPSR in copepods approaching the cylinder (triangles) and drifting within the cylinder wake (circles).
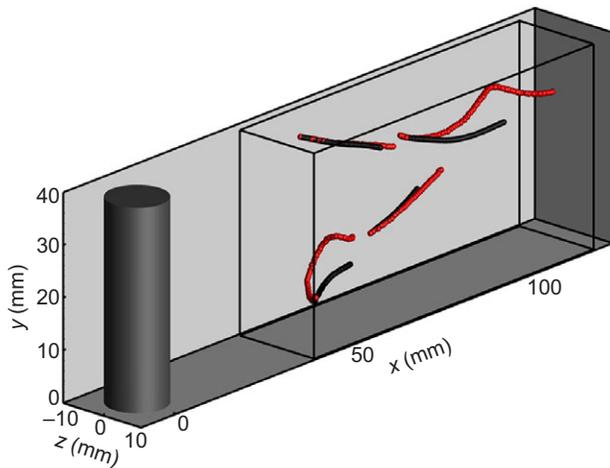
Fig. 6. 3D trajectories of copepods and passive fluid 'particles'. 3D trajectories of four copepods (red) compared with passive fluid 'particles' (black), where each fluid particle was initialized at initial copepod location and propagated according to the local fluid velocity.

The fluid particle trajectories (Fig. 6) deviate from the zooplankton trajectories, suggesting that inertial drift of the copepods can be surprisingly significant in unsteady or turbulent flow fields. Note that the trajectory differences cannot be explained by measurement uncertainty (Appendix 1). The current method can directly determine inertial drift or slip of zooplankton or other organisms. Such results can be used to help predict drift and aggregation in the ocean or other fluid environments. See Appendix 2 for extensions and applications of the measurement system.

Appendix 1
Contribution of measurement uncertainty to slip velocity and fluid particle trajectory
For tomographic PIV, the uncertainty of displacement was 0.3 voxels to 97% confidence level, which implies uncertainty of an individual fluid velocity vector as 0.003 m s^{-1} ($\sim$0.04U_0) for a freestream velocity of U_0=0.077 m s^{-1}. For 3D PTV, uncertainty of the zooplankton location was estimated as 0.04 mm (or 0.5 voxel) in x and y directions, and 0.07 mm (or 0.86 voxel) in the z direction, again to 97% confidence level. This translates to velocity uncertainties of 0.006 m s^{-1} ($\sim$0.06U_c) in x and y directions and 0.01 m s^{-1} ($\sim$0.1U_c) in the z direction, where U_c=0.1 m s^{-1} is the typical maximum velocity of an escaping copepod.

Slip velocity
Measurement uncertainty can contribute to the apparent slip velocity of copepods within moving fluids. We show that the difference between zooplankton velocity and the local fluid velocity shown in Fig. 3B is indeed a result of an actual slip velocity, and not due to uncertainty associated with their measurement.

Table A1 shows the Cartesian velocity components of the zooplankton, the local fluid, and their uncertainties (Δ) for the vectors in Fig. 3B.

From Table A1, we note that the values of u and w (i.e. x- and z-component velocities) of the zooplankton and local fluid element

are similar within the limits of uncertainty. However, the value of v (y-component velocity) for zooplankton and local fluid velocity differs significantly. This slip velocity in the y component is calculated to be 0.014±0.007 m s^{-1}, which is clearly larger than the uncertainty, thus, the different vectors in Fig. 3B must result from interactive forces between the zooplankton and the surrounding unsteady flow field.

Fluid particle trajectory
Fig. 6 shows a clear deviation of zooplankton and the non-inertial fluid particle trajectory. Propagation of measurement uncertainty during particle trajectory computation may contribute to this deviation. We will show that this propagation of uncertainty is very low compared with the final location differences between non-inertial particle and zooplankton. The uncertainty of fluid 'particle' trajectory can be formulated as follows:

Let x_0 be the x component of the initial location of the fluid particle and the zooplankton (Fig. A1). The x-component velocity of the fluid particle at certain space and time in its trajectory is given as $u_i(x_i,t_i)$. For instance, at x_0 the velocity of fluid particle is $u_0(x_0,0)$. Particle trajectory is computed using the measured time-series fluid velocity field that is separated by a short time interval of Δt. Given a particle is at x_i, we can compute x_{i+1} using the first order Taylor-series expansion:

$$x_{i+1} = x_i + u_i \Delta t. \tag{A1}$$

Therefore, for a trajectory of the fluid particle starting at x_0 and traveling over p time intervals, we can compute the final x location, x_p, of the particle is as follows:

$$x_p = x_0 + \Delta t \sum_{i=0}^{p-1} u_i. \tag{A2}$$

Given the measured uncertainty in the x component of the local fluid velocity (Δu), the uncertainty in the final location (Δx_p) of the particle will be:

$$\Delta x_p = \sqrt{(\Delta t)^2 \sum_{i=0}^{p-1} (\Delta u_i)^2 + (\Delta x_0)^2}. \tag{A3}$$

The form of Eqn A3 is also valid for the y and z components (i.e. Δy_p, Δz_p), although the actual uncertainty Δz_0 is larger than Δx_0 and Δy_0. Based on Fig. 6, the number of time steps is p=98, the uncertainty in local fluid velocity for all components is 0.003 m s^{-1}, and the time interval is Δt=3 ms. Therefore, the uncertainties in the final x, y and z locations based on the above equation are (Δx_p, Δy_p, Δz_p)=(0.10 mm, 0.10 mm, 0.11 mm).

Considering these uncertainties and the final separation distances between the copepods and initialized fluid particles (Table A2), which are significantly larger, we conclude that the separate trajectories cannot result from measurement uncertainty.

Appendix 2
Extensions and applications of infrared tomographic PIV+3D PTV method
For the current method, the volumetric velocity field has a small-scale cubic grid size of 0.9 mm and large-scale measurement

Table A1. Velocity components and their corresponding uncertainty (97% confidence level) for zooplankton and local fluid velocities

	u (m s^{-1})	Δu (m s^{-1})	v (m s^{-1})	Δv (m s^{-1})	w (m s^{-1})	Δw (m s^{-1})
Zooplankton velocity	0.049	±0.006	0.011	±0.006	−0.004	±0.01
Local fluid velocity	0.052	±0.003	−0.003	±0.003	−0.008	±0.003
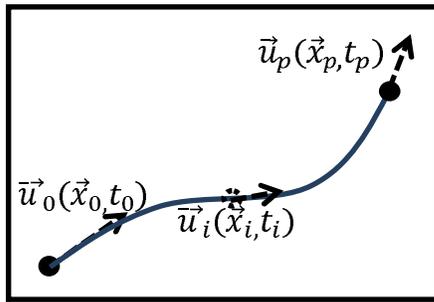
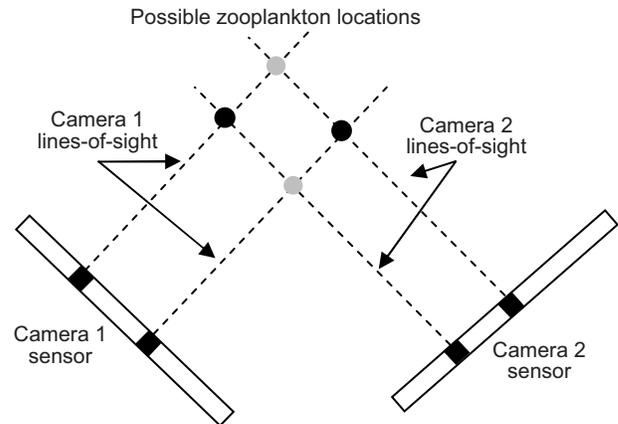**Fig. A1. Schematic diagram of the fluid particle trajectory within a fluid velocity field.**

Fig. A2. Schematic representation of reconstruction ambiguity. Cameras 1 and 2 each show two plankton images as black spots. Since neither of the cameras can identify the specific plankton, their volumetric location and number is ambiguous. Possible solutions include only two plankton (depicted by black or gray circles) any three plankton or all four plankton present in the volume.

volume size of 80 mm×37.5 mm×19 mm. This spatial range (i.e. range between measurement volume and grid size) is not limited by the method, but by the tomographic PIV camera hardware capabilities (i.e. the number of pixels and sensor size). Larger spatial range could be obtained by increasing the number of pixels in the camera sensor array or by decreasing the interrogation volume within tomographic PIV. Decreasing interrogation volume would necessitate increased density of seeding particles or improvements in reconstruction software. A larger z dimension can be attained by increasing illumination thickness. Assuming the current software, additional cameras may be required to maintain volume reconstruction quality if more seeding particles are added or the illumination volume thickness is increased (Elsinga et al., 2006; Scarano, 2013).

For 3D PTV used in the current method, the number of copepods within the measurement volume at any given time was 7(±3). If the number increases, the chance of identifying ambiguous individuals also increases. Ambiguities occur during volumetric reconstruction when there are multiple candidates for a possible object location. This may be a consequence of either a line-of-sight from one camera intersecting multiple organisms on another camera image, or overlapping organisms in one or more camera views. Fig. A2 shows a simple 2D schematic representation of the ambiguity problem based on recordings by two 1D camera sensor arrays. The figure shows that the two zooplankton detected by both cameras 1 and 2 satisfy more than one possible configuration in the volume (e. g. 2 black circles, 2 gray circles, any 3 circles or all 4 circles). Maas (1992) formulated an equation for the expected number of ambiguities in a two-camera 3D PTV arrangement. Based on this equation, one copepod location of every 200 measured would be ambiguous for the current experiment. It should be noted that the number of ambiguities grows approximately with the square of the organism number density, linearly with the length of the line-of-sight within the volume, and linearly with triangulation error (Maas, 1992). An additional PTV camera can be added or images from additional time steps can be employed (e.g. Schanz et al., 2014) to reduce this ambiguity problem.

The ability to track 3D copepod trajectory within volumetric flow fields will allow greater insight into how this ecologically important group responds to complex fluid environments. This has

Table A2. Final distance between the copepods and fluid particles for *x*, *y* and *z* components

	$\lvert x_{plankton}-x_{tracer}\rvert$ (mm)	$\lvert y_{plankton}-y_{tracer}\rvert$ (mm)	$\lvert z_{plankton}-z_{tracer}\rvert$ (mm)
1	2.72	0.22	1.00
2	20.25	1.08	6.35
3	4.05	7.72	4.95
4	6.75	1.94	0.14

implications for understanding the role of small-scale eddies and other flow structures in altering copepod abundance at oceanographic fronts, near coral reefs, during diel vertical migration and interactions with predators. This measurement technique can be extended easily to study other organisms found in the ocean or freshwater bodies. Examples include motile or inertial phytoplankton, other zooplanktons (e.g. krill, pteropods, etc.) and even fish schools. With its capability to identify and track multiple organisms and measure complex flow variations in a volumetric domain, this technique can provide measurement means for researchers interested in biogenic mixing (Katija and Dabiri, 2009), *in situ* characterization of organisms and flow (Sutherland et al., 2011), krill schooling (Catton et al., 2011), plankton aggregation in oceanic thin layers (Durham and Stocker, 2012) or predator–prey interactions (Buskey et al., 2002; Adhikari, 2013; Rothschild and Osborn, 1988). Thus, the application of this technique can extend from investigating organism movement within benthic boundary layers to even wind-driven seed dispersal in terrestrial systems. Furthermore, with ongoing improvements in the velocimetry algorithms (e.g. 'Shake the box' method by Schanz et al., 2014), measurements of even larger ranges of scale and organism number density would be possible.

Unless we are able to measure 3D trajectories and fluid velocity variations simultaneously, our understanding of plankton motion and response within turbulent or other complex flows will remain limited. Since fluid and plankton motion in the environment are not only 3D but also time-varying, they typically cannot be determined or predicted based on simplifying assumptions or planar measurements. This motivated development of the current method, which although relatively complicated to implement, nevertheless enables exploration of various sensory and locomotive aspects of organisms, complex fluid dynamics, and their interactions. Moreover, both smaller-scale interactions and larger-scale spatial distribution and trajectories of organisms can be studied simultaneously. Thus, the capabilities of the method described can be used to address many unresolved questions regarding animal–fluid interactions in the biology community.

References
Adhikari, D. (2013). Volumetric Velocity Measurement of Predator-prey Interactions. *PhD thesis*, University of Minnesota, MN.
Adhikari, D. and Longmire, E. K. (2013). Infrared tomographic PIV and 3D motion tracking system applied to aquatic predator–prey interaction. *Meas. Sci. Technol.* **24**, 024011.
Atkinson, C. and Soria, J. (2009). An efficient simultaneous reconstruction technique for tomographic particle image velocimetry. *Exp. Fluids* **47**, 553-568.
Buskey, E. J., Lenz, P. H. and Hartline, D. K. (2002). Escape behavior of planktonic copepods in response to hydrodynamic disturbances: high speed video analysis. *Mar. Ecol. Prog. Ser.* **235**, 135-146.
Catton, K. B., Webster, D. R., Kawaguchi, S. and Yen, J. (2011). The hydrodynamic disturbances of two species of krill: gait kinematics and system design. *Mar. Biol.* **158**, 2541-2554.
Catton, K. B., Webster, D. R. and Yen, J. (2012). The effect of fluid viscosity, habitat temperature, and body size on the flow disturbance of Euchaeta. *Limnol. Oceanogr.* **2**, 80-92.
Durham, W. M. and Stocker, R. (2012). Thin phytoplankton layers: characteristics, mechanisms and consequences. *Annu. Rev. Mar. Sci.* **4**, 177-207.
Durham, W. M., Climent, E., Barry, M., De Lillo, F., Boffetta, G., Cencini, M. and Stocker, R. (2013). Turbulence drives microscale patches of motile phytoplankton. *Nat. Commun.* **4**, 2148.
Elsinga, G. E., Scarano, F., Wieneke, B. and van Oudheusden, B. W. (2006). Tomographic particle image velocimetry. *Exp. Fluids* **41**, 933-947.
Fields, D. M. and Yen, J. (1997). The escape behavior of marine copepods in response to a quantifiable fluid mechanical disturbance. *J. Plankton Res.* **19**, 1289-1304.
Flammang, B. E., Lauder, G. V., Troolin, D. R. and Strand, T. E. (2011). Volumetric imaging of fish locomotion. *Biol. Lett.* **7**, 695-698.
Gemmell, B. J., Sheng, J. and Buskey, E. J. (2013). Compensatory escape mechanism at low Reynolds number. *Proc. Natl. Acad. Sci. USA* **110**, 4661-4666.
Gemmell, B. J., Adhikari, D. and Longmire, E. K. (2014). Volumetric quantification of fluid flow reveals fish's use of hydrodynamic stealth to capture evasive prey. *J. R. Soc. Interface* **11**, 20130880.
Gemmell, B. J., Troolin, D. R., Costello, J. H., Colin, S. P. and Satterlie, R. A. (2015). Control of vortex rings for manoeuvrability. *J. R. Soc. Interface* **12**, 20150389.
Gilbert, O. M. and Buskey, E. J. (2005). Turbulence decreases the hydrodynamic predator sensing ability of the calanoid copepod *Acartia tonsa*. *J. Plankton Res.* **27**, 1067-1071.
Guasto, J. S., Rusconi, R. and Stocker, R. (2012). Fluid mechanics of planktonic microorganisms. *Annu. Rev. Fluid Mech.* **44**, 373-400.

Haury, L. R., Kenyon, D. E. and Brooks, J. R. (1980). Experimental evaluation of the avoidance reaction of *Calanus finmarchicus*. *J. Plankton Res.* **2**, 187-202.
Holzman, R. and Wainwright, P. C. (2009). How to surprise a copepod: Strike kinematics reduce hydrodynamic disturbance and increase stealth of suction-feeding fish. *Limnol. Oceanogr.* **54**, 2201-2212.
Jiang, H. and Kiørboe, T. (2011). Propulsion efficiency and imposed flow fields of a copepod jump. *J. Exp. Biol.* **214**, 476-486.
Jumars, P. A., Trowbridge, J. H., Boss, E. and Karp-Boss, L. (2009). Turbulence-plankton interactions: a new cartoon. *Mar. Ecol.* **30**, 133-150.
Katija, K. and Dabiri, J. O. (2009). A viscosity-enhanced mechanism for biogenic ocean mixing. *Nature* **460**, 624-626.
Kiørboe, T., Saiz, E. and Visser, A. (1999). Hydrodynamic signal perception in the copepod *Acartia tonsa*. *Mar. Ecol. Prog. Ser.* **179**, 97-111.
Krizan, D. (2014). Copepod response behavior in turbulence. M.Sc. thesis. University of Minnesota, MN.
Maas, H. G. (1992). Complexity analysis for the determination of image correspondences in dense spatial target fields. *Int. Arch. Photogramm. Remote Sens.* **XXIX**, 102-107.
Maas, H. G., Gruen, A. and Papantoniou, D. (1993). Particle tracking velocimetry in three-dimensional flows. Part 1. Photogrammetric determination of particle coordinates. *Exp. Fluids* **15**, 133-146.
Malkiel, E., Sheng, J., Katz, J. and Strickler, J. R. (2003). The three-dimensional flow field generated by a feeding calanoid copepod measured using digital holography. *J. Exp. Biol.* **206**, 3657-3666.
Mauchline, J. (1998). *The Biology of Calanoid Copepods*. San Diego, CA: Academic Press.
Maxey, M. R. and Riley, J. J. (1983). Equation of motion for a small rigid sphere in a nonuniform flow. *Phys. Fluids* **26**, 883.
Michaelis, D. (2014). Time resolved volumetric visualization of zooplankton body and surrounding flow field using advanced masking in tomographic PIV. 16th Int Symp on Flow Visualization. Okinawa, Japan.
Miller, C. B. (2004). *Biological Oceanography*. Malden, MA: Blackwell Publishing Company.
Murphy, D. W., Webster, D. R. and Yen, J. (2012). A high speed tomographic PIV system for measuring zooplankton flow. *Limnol. Oceanogr.* **10**, 1096-1112.
Prairie, J. C., Sutherland, K. R., Nickols, K. J. and Kaltenberg, A. M. (2012). Biophysical interactions in the plankton: a cross-scale review. *Limnol. Oceanogr.* **2**, 121-145.
Robinson, H. E., Finelli, C. M. and Buskey, E. J. (2007). The turbulent life of copepods: effects of water flow over a coral reef on their ability to detect and evade predators. *Mar. Ecol. Prog. Ser.* **349**, 171-181.
Rothschild, B. J. and Osborn, T. R. (1988). Small-scale turbulence and plankton contact rates. *J. Plankton Res.* **10**, 465-474.
Scarano, F. (2013). Tomographic PIV: principles and practice. *Meas. Sci. Technol.* **24**, 012001.
Schanz, D., Schroder, A., Gesemann, S. (2014). 'Shake The Box' - a 4D PTV algorithm: Accurate and ghostless reconstruction of Lagrangian tracks in densely seeded flows. 17th Int. Symp. Appl. of Laser Techniques to Fluid Mechanics, Lisbon, Portugal.
Sutherland, K. R., Dabiri, J. O. and Koehl, M. A. R. (2011). Simultaneous field measurements of ostracod swimming behavior and background flow. *Limnol. Oceanogr.* **1**, 135-146.
Wieneke, B. (2008). Volume self-calibration for 3D particle image velocimetry. *Exp. Fluids* **45**, 549-556.
Woodson, C. B., Webster, D. R., Weissburg, M. J. and Yen, J. (2005). Response of copepods to physical gradients associated with structure in the ocean. *Limnol. Oceanogr.* **50**, 1552-1564.
Woodson, C. B., Webster, D. R., True, A. C. (2014). Copepod behavior: oceanographic cues, distributions and trophic interactions. In *Copepods: Diversity, Habitat and Behavior* (ed. L. Seuront), pp. 215–253. Nova Sci Pub.
Yamazaki, H. and Squires, K. D. (1996). Comparison of oceanic turbulence and copepod swimming. *Mar. Ecol. Prog. Ser.* **144**, 299-301.
Yen, J. (2000). Life in transition: balancing inertial and viscous forces by planktonic copepods. *Biol. Bull.* **198**, 213-224.
Yen, J., Rasberry, K. D. and Webster, D. R. (2008). Quantifying copepod kinematics in a laboratory turbulence apparatus. *J. Mar. Sys.* **69**, 283-294.